Int. J. Heat Mass Transfer. Vol. 34, No. 2, pp. 461–471, 1991
Printed in Great Britain

0017–9310/91 $3.00 + 0.00
© 1991 Pergamon Press plc

Double diffusive natural convection in a vertical rectangular enclosure—II. Numerical study

HWATAIK HAN and THOMAS H. KUEHN
Department of Mechanical Engineering, University of Minnesota, Minneapolis, MN 55455, U.S.A.

(*Received* 28 *December* 1989 *and in final form* 6 *April* 1990)

Abstract—A numerical study is performed on double diffusive natural convection fluid flow in a vertical rectangular cavity of aspect ratio 4 when the temperature and concentration gradients are imposed in the horizontal direction. A finite difference algorithm is adopted to solve the non-linear momentum equations coupled with the energy and concentration equations. Double diffusive multicell flow structures observed in experiments by the authors are simulated successfully. Different flow structure regimes are obtained as a function of the Grashof number ratio for aiding and opposing buoyancy conditions.

1. INTRODUCTION

THIS PAPER considers double diffusive natural convection when horizontal temperature and concentration gradients coexist in a rectangular cavity. The natural convection induced by simultaneous heat and mass transfer is often referred to as double diffusive convection when the Lewis number is considerably different from unity. Double diffusive convection frequently occurs in oceans, magma chambers, as well as in many engineering applications such as solar ponds, natural gas storage tanks, crystal manufacturing, and metal solidification processes. Unique double diffusive convection phenomena, such as salt fingers and diffusive interfaces have been observed due to the significant difference in diffusivities of heat and mass [1].

There are many convection modes depending on the directions of temperature and concentration gradients relative to gravity, as pointed out by Ostrach [2]. Most of the initial theoretical studies on double diffusive convection have been performed for vertical temperature and concentration gradients for ocean applications using linear stability theory [1]. Similar configurations have been studied numerically to simulate the complicated, sometimes chaotic, mantle movement in the earth's crust [3]. The problem can be considered as an extension of Benard convection cells. A finite element scheme has been applied [4] to simulate the layered fluid structures observed in experiments on lateral heating in a stably salt-stratified fluid [5]. It was found that stability theory can predict the initial stage of the transient process. These configurations, either lateral heating or bottom heating, are inherently transient, as the initial salt stratification disappears.

Beckermann and Viskanta [6] simulated double diffusive layers occurring in a solidification process when a horizontal temperature gradient is present. Considerable discrepancies between numerical solutions and experimental measurements were reported because of the complicated solidification process, which involves phase changes and non-stationary irregular interfaces. When horizontal temperature and concentration gradients are present in a simple rectangular enclosure, steady-state solutions were obtained by Hu and El-Wakil [7] and more recently by Benard *et al.* [8]. The flow structure obtained was a unicell flow structure similar to pure heat transfer convection, since the Lewis number considered was not much different from unity. Recent experiments on double diffusive convection have exhibited multicell flow structures for horizontal temperature and concentration gradients in an enclosed cavity [9, 10]. No references, however, have been found which simulate steady-state double diffusive convection cells in a simple rectangular enclosure geometry using a numerical technique. The difficulty lies in the large values for the Lewis and Grashof numbers, which makes it difficult to obtain a converged solution.

The main purpose of this study is to simulate the double diffusive multicell flow structures observed in an experimental study by the present authors [11, 12]. Both aiding and opposing buoyant conditions are considered in a cavity of aspect ratio 4. The Prandtl and the Schmidt numbers are set at 8 and 2000, respectively, which approximate the experimental values. The Grashof number range studied in the experiments is extended over a wider range. Thermal Grashof numbers vary from -4×10^5 to 3×10^5 for a solutal Grashof number fixed at 10^5 and 3×10^6. Comprehensive information on velocity, temperature, and concentration distributions in a cavity are presented and are compared with the experimental results.

2. MATHEMATICAL FORMULATION

A schematic diagram of the present problem is shown in Fig. 1. Depending on the directions of the buoyant forces, the problem can be either an aiding or

NOMENCLATURE

C	molar concentration of cupric ions [mol l^{-1}]
c	dimensionless concentration, $(C-C_{low})/(C_{high}-C_{low})$
D	diffusion coefficient of cupric ions in aqueous solution [$m^2\ s^{-1}$]
g	gravitational acceleration [m s^{-2}]
Gr_M	solutal Grashof number, $g\beta_m\Delta CH^3/v^2$
Gr_T	thermal Grashof number, $g\beta_t\Delta TH^3/v^2$
H	height of the enclosure [m]
h	heat transfer coefficient [W $m^{-2}\ °C^{-1}$]
h_m	mass transfer coefficient [m s^{-1}]
k	thermal conductivity [W $m^{-1}\ °C^{-1}$]
L	width of the enclosure [m]
Le	Lewis number, Sc/Pr
$L1$	number of grids in the x-direction
$M1$	number of grids in the y-direction
N	buoyancy ratio, $\beta_m\Delta C/\beta_t\Delta T$ or Gr_M/Gr_T
Nu	Nusselt number, hH/k
P	pressure
Pr	Prandtl number, v/α
Sc	Schmidt number, v/D
Sh	Sherwood number, h_mH/D
T	temperature [°C]
t	dimensionless temperature, $(T-T_{cold})/(T_{hot}-T_{cold})$
U	horizontal velocity [m s^{-1}]
V	vertical velocity [m s^{-1}]
X	horizontal coordinate [m]
Y	vertical coordinate [m].

Greek symbols

α	thermal diffusivity [$m^2\ s^{-1}$]
β_m	solutal volumetric expansion coefficient [l mol^{-1}]
β_t	thermal volumetric expansion coefficient [$°C^{-1}$]
v	kinematic viscosity [$m^2\ s^{-1}$]
ρ	density [kg m^{-3}]
ψ	stream function.

opposing buoyancy condition. The solutal boundary layer is considered to be thinner than the thermal boundary layer since the solutal diffusivity is much smaller than the thermal diffusivity.

The flow in the cavity is considered to be two-dimensional and steady, and follows classical Boussinesq approximation. The fluid is assumed to be incompressible and Newtonian in behavior with negligible viscous dissipation. The heat flux driven by concentration gradients (thermal diffusion or Soret effect) and the mass flux driven by temperature gradients (diffusion thermo or Dufour effect) are neglected. By employing the above assumptions into the conservation equations of mass, momentum, energy, and species, a set of governing equations is obtained as

$$\frac{\partial u}{\partial x}+\frac{\partial v}{\partial y}=0 \tag{1}$$

$$u\frac{\partial u}{\partial x}+v\frac{\partial u}{\partial y}=-\frac{\partial p}{\partial x}+\left(\frac{\partial^2 u}{\partial x^2}+\frac{\partial^2 u}{\partial y^2}\right) \tag{2}$$

$$u\frac{\partial v}{\partial x}+v\frac{\partial v}{\partial y}=-\frac{\partial p}{\partial y}+\left(\frac{\partial^2 v}{\partial x^2}+\frac{\partial^2 v}{\partial y^2}\right)+(Gr_T\,t+Gr_M\,c) \tag{3}$$

$$u\frac{\partial t}{\partial x}+v\frac{\partial t}{\partial y}=\frac{1}{Pr}\left(\frac{\partial^2 t}{\partial x^2}+\frac{\partial^2 t}{\partial y^2}\right) \tag{4}$$

$$u\frac{\partial c}{\partial x}+v\frac{\partial c}{\partial y}=\frac{1}{Sc}\left(\frac{\partial^2 c}{\partial x^2}+\frac{\partial^2 c}{\partial y^2}\right). \tag{5}$$

The above equations have been made dimensionless using the following parameters:

$$x=\frac{X}{H},\quad y=\frac{Y}{H},\quad u=\frac{U}{v/H},\quad v=\frac{V}{v/H},$$

$$p=\frac{P}{\rho v^2/H^2},\quad t=\frac{T-T_{cold}}{T_{hot}-T_{cold}},\quad C=\frac{C-C_{low}}{C_{high}-C_{low}}. \tag{6}$$

The dimensionless boundary conditions for the physical system considered in the present study are

at $x=0$; $c=0, t=1$ (aiding)

$t=0$ (opposing)

at $x=\frac{L}{H}$; $c=1, t=0$ (aiding)

$t=1$ (opposing)

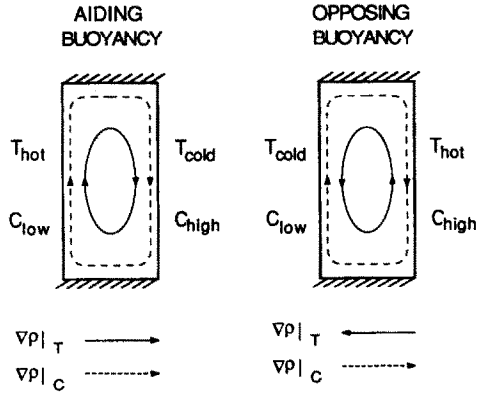

FIG. 1. Schematic drawings of the present problem.

$$\frac{\partial t}{\partial y} = \frac{\partial c}{\partial y} = 0 \quad \text{at } y = 0 \text{ and } 1$$

$$u = v = 0 \quad \text{at } x = 0, \frac{L}{H} \quad \text{and at } y = 0, 1. \quad (7)$$

Horizontal velocity of the bulk fluid at the vertical surfaces due to the cupric ion transfer is found to be negligible. The concentration of cupric ions on a cathode is zero at a limiting current condition. The concentration of the cupric ions on the anode surface is considered to be twice the bulk concentration by assuming symmetry of the cathode and anode [11].

For aiding buoyancy conditions, the vertical hot surface is maintained at a low concentration, while the cold surface is maintained at a high concentration. For opposing buoyancy conditions, this is reversed. In actual programming, a buoyancy force acting in the reverse direction is implemented by changing the sign of the thermal Grashof number in equation (3) instead of changing the values of the boundary conditions.

3. SOLUTION PROCEDURE

Finite difference equations are derived by integrating the governing differential equations over an elementary control volume. A power law scheme is adopted for the convection–diffusion formulation. The coupling between the non-linear algebraic equations is handled using the SIMPLER algorithm [13]. The discretized equations obtained are solved iteratively, using a line-by-line application of the Thomas algorithm. The non-linear coefficients are substituted successively with updated values. Underrelaxation is required to ensure the convergence of the iterative procedure, and a block correction scheme is incorporated to accelerate the convergence rate.

Non-uniform grid spacing is used in the x-direction. Grid spacing is minimum near a vertical wall and is increased exponentially away from the wall up to the center of the cavity according to the following expression:

$$XU(i) = \left[\frac{i-2}{\frac{L1}{2}-2}\right]^2 \quad (8)$$

where $XU(i)$ are the locations of control volume faces, and $L1$ is the number of grids in the x-direction. Uniform mesh spacing is used in the y-direction in order to resolve the possible multicell flow structure. Since the location of the cell interfaces are not known a priori, fine meshes are required everywhere in the vertical direction. Typical numbers of grids used are 34×130 in the x- and y-directions, respectively.

The solution is considered to be fully converged when the maximum value of the mass source and the changes of the dependent variables from iteration to iteration are smaller than a prescribed value, i.e. 10^{-5}. Due to the small solutal diffusivity of the fluid, the convergence rate is very slow, especially for solutal buoyancy dominant flows. A typical number of iterations to obtain a fully converged solution is approximately 1000 for simple flows, and more than 5000 for complex flows. Most of the runs have been made on a Cray-2 supercomputer with four processors at the University of Minnesota Supercomputer Institute. The CPU time for calculating 1000 iterations for a 34×130 grid is approximately 10 min.

Nusselt and Sherwood numbers are calculated after convergence is attained. The local Nusselt number at the wall is defined as

$$Nu(y) = \frac{hH}{k} = -\left.\frac{\partial t}{\partial x}\right|_{\text{wall}}. \quad (9)$$

The non-dimensional temperature gradients are calculated by assuming a linear temperature profile between grids. The local Nusselt numbers are integrated to obtain an overall average Nusselt number for the cavity. An overall Nusselt number in the middle of the cavity can be calculated by adding a convection term to the diffusion term. It is within 0.5% of the Nusselt number determined at the wall. The difference between them is an indication of the convergence and the correctness of the finite difference approximation.

Similar equations can be applied in calculating the Sherwood numbers. The local Sherwood number at a wall is expressed as

$$Sh(y) = \frac{h_m H}{D} = -\left.\frac{\partial c}{\partial x}\right|_{\text{wall}}. \quad (10)$$

The average Sherwood numbers are obtained by integrating the local values in the y-coordinate direction. The average values at the two vertical walls are identical.

4. RESULTS AND DISCUSSION

4.1. *Test of grid dependence*

In order to validate the present numerical code, and to report the error range of the results, preliminary numerical aspects are presented first. Pure heat transfer solutions obtained for $Ra = 10^3$–10^6, $Pr = 0.71$ in a square cavity have been compared with the benchmark results of de Vahl Davis [14]. The average Nusselt numbers using second-order polynomials extrapolated to zero grid size are within 1% of the benchmark results. Pure heat transfer solutions for a high Prandtl number fluid ($Pr = 2000$, $Ra = 10^5$, $H/L = 4$) have also been obtained by varying the grid spacing in each direction independently ($L1 = 22$–52, $M1 = 34$–130). The average Nusselt numbers can be found in ref. [12]. The results show that the number of grid points in the x-direction should be larger than 22 and the number of grid points in the y-direction should be larger than 82 in order to maintain the

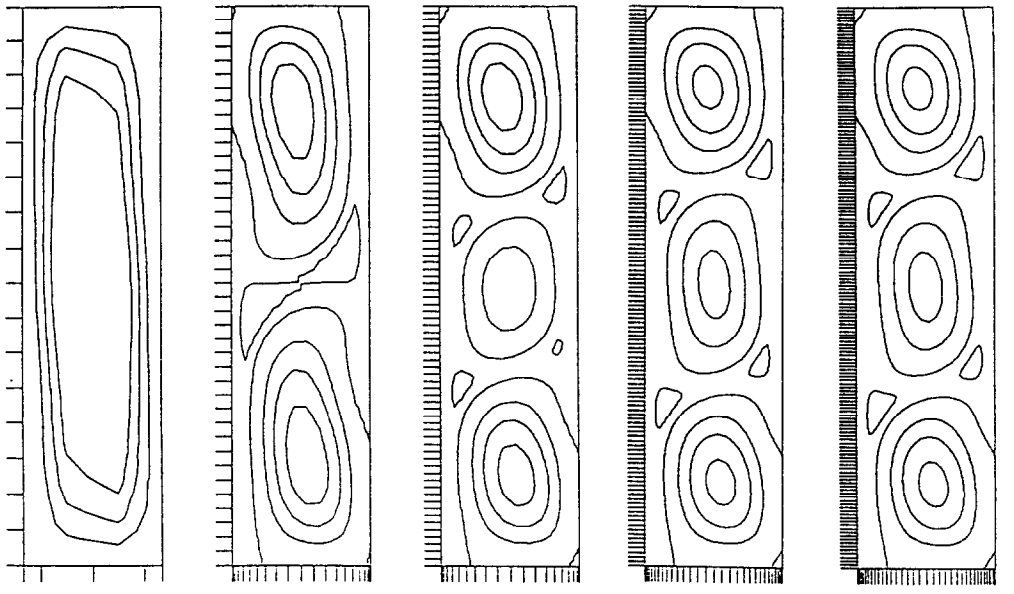

FIG. 2. Effect of grid spacing on converged solution flow structure: $Gr_T = -2 \times 10^4$, $Gr_M = 10^5$.

discretization error within 1% for the present range of parameters.

Various streamline patterns of converged solutions are obtained as shown in Fig. 2 depending on the number of grids for simultaneous heat and mass transfer, $Gr_T = -2 \times 10^4$, $Gr_M = 10^5$, $Pr = 8$, $Sc = 2000$, $H/L = 4$. It is interesting to note that the grid spacing affects the converged flow pattern as well as the accuracy of the overall heat and mass transfer rates. A three cell flow structure is obtained with fine grid spacings. The grids coarser than 22×82 are not able to resolve the thin shear layers between cells. The maximum value of stream function obtained at 34×130 is within 1% of that obtained at 42×162. The overall Nusselt and Sherwood numbers obtained at those grid spacings match up to three digits. In order to compromise between computational cost and accuracy, a grid of 34×130 is used for most runs except obvious simple unicell flow structures. Furthermore, it is recommended that the average grid size in both coordinate directions should be of the same order of magnitude to ensure convergence.

4.2. *Multicell flow structure and comparison with experiments*

Figure 3 shows plots of velocity vectors, streamlines, isotherms and isoconcentration contours of the converged solution for an opposing buoyancy condition: $Gr_T = -4 \times 10^5$, $Gr_M = 3 \times 10^6$. The three cell structure is obtained as was observed in the corresponding experiment [11]. The velocity vectors indicate that the fluid inside the thin concentration boundary layers moves against the bulk fluid motion in the counter-clockwise direction driven by thermal buoyancy in the core. However, the direction of the fluid motion in the concentration boundary layer does not appear to effect the overall fluid motion in the core region significantly. There are high shear regions near the concentration boundary layer edges due to the bidirectional flows. This type of velocity pattern has not been observed in single diffusive convection flows. Figures 3(c) and (d) show that the temperature field is stably stratified in each cell, and that the concentration is nearly uniform in each cell except near the walls and cell interfaces. The cross-sectional temperature and concentration profiles along the vertical centerline are shown in Fig. 4 in comparison with corresponding experimental results. The temperature profile measured in the bottom cell shows quite a discrepancy with the predicted result. The discrepancy is believed to be partly due to non-uniform properties of the fluid because of the temperature and concentration gradients and partly due to the assumption of the constant concentration boundary condition on the anode surface. An additional explanation for the non-symmetry of the measurements is given in ref. [11].

A three cell flow structure is also obtained for an aiding buoyancy condition: $Gr_T = 3 \times 10^5$, $Gr_M = 3 \times 10^6$. The basic overall flow structure is similar to the previous opposing buoyancy condition, even though the details are not the same. The cross-sectional vertical velocity profile does not show a bidirectional behavior in the boundary layers. The temperature and concentration profiles are similar to those of the previous opposing buoyancy case. The calculated

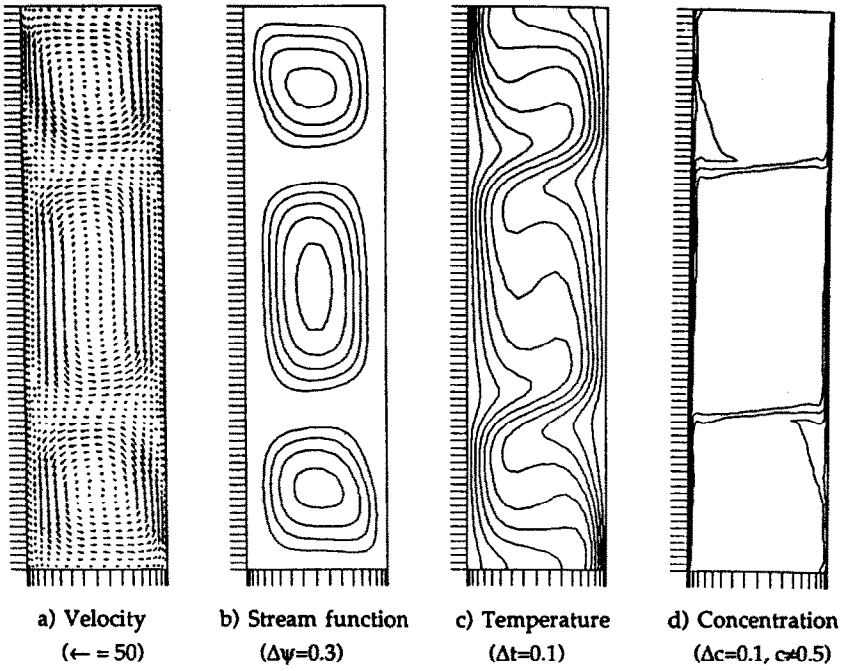

FIG. 3. Velocity vectors, streamlines, isotherms and iso-concentration contours for an opposing buoyancy solution: $Gr_T = -4 \times 10^5$, $Gr_M = 3 \times 10^6$.

concentration distribution is compared with a still photograph taken through the experimental cavity in Fig. 5. The cupric ion has a blue color, and the darkness of the color determines the concentration of cupric ion in the solution.

The local Nusselt number distribution along the vertical heated wall, where the concentration is zero, is shown in Fig. 6(a). The Nusselt number shows local maximums and minimums along the wall as was found in the opposing buoyancy condition. The maximums occur where the fluid flows toward the wall, and the minimums occur where the fluid flows away from the wall. Figure 6(b) shows the local Sherwood number distribution along the wall in comparison with the experimental results. The Sherwood number distribution appears to be nearly monotonically decreasing with respect to the vertical coordinate. The mass transfer rate appears to be less affected

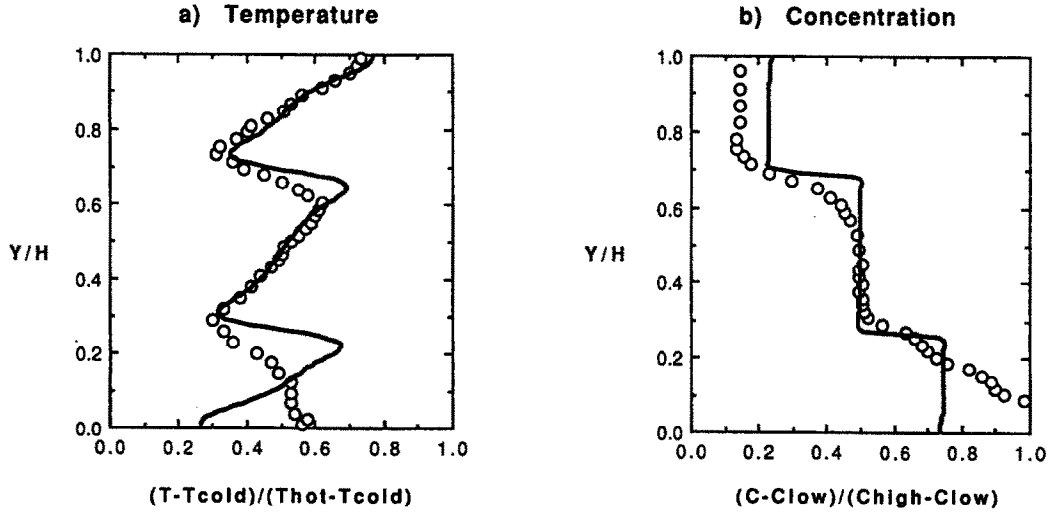

FIG. 4. Temperature and concentration distributions along the vertical centerline: $Gr_T = -4 \times 10^5$, $Gr_M = 3 \times 10^6$ (solid curves are numerical results, and symbols are experimental data).

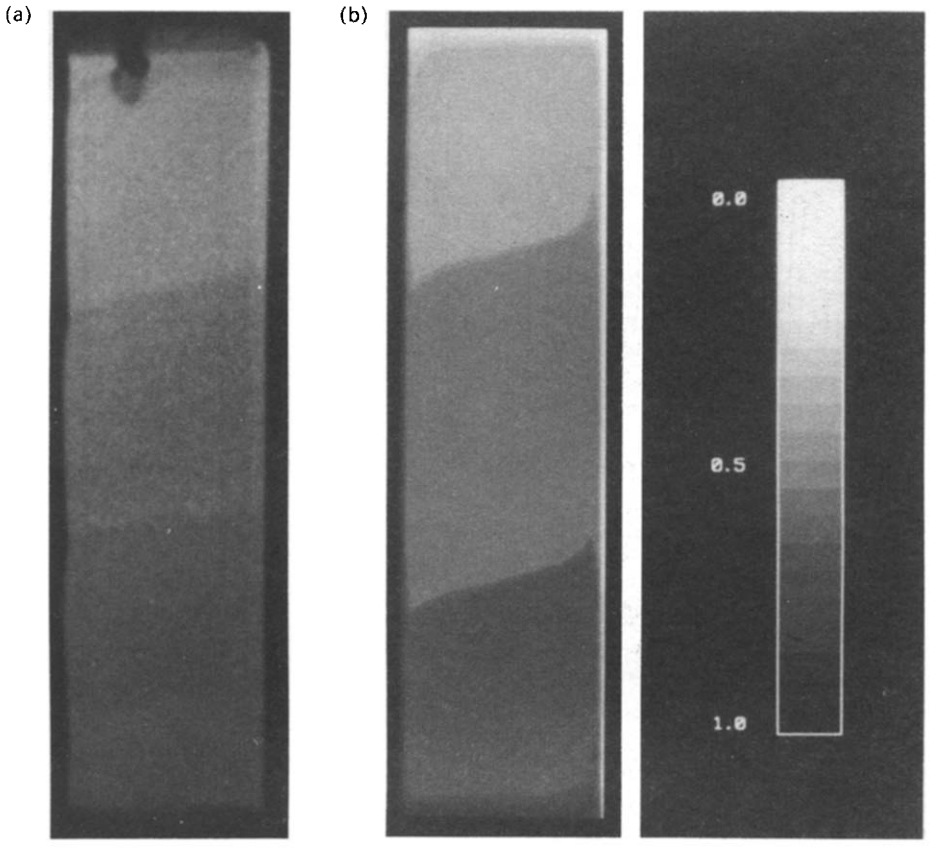

FIG. 5. Comparisons of concentration distributions in the cavity for aiding buoyancy (fluid rotates counterclockwise in each cell). (a) Experiment ($N = 8.5$, $Le = 280$): $Gr_T = 3.8 \times 10^5$, $Pr = 8.5$; $Gr_M = 3.2 \times 10^6$, $Sc = 2400$. (b) Calculation ($N = 10$, $Le = 250$): $Gr_T = 3.0 \times 10^5$, $Pr = 8.0$; $Gr_M = 3.0 \times 10^6$, $Sc = 2000$.

by the presence of the multiple cells in the core than the heat transfer rate, since the concentration gradients are mostly confined within the thin concentration boundary layers regardless of aiding or opposing buoyancy conditions. The discrepancy in simulating the double diffusive convection experiments may be due to the assumption of constant properties, especially the viscosity and the diffusion coefficients. It may also be due to non-uniform concentration boundary conditions on the electrode sur-

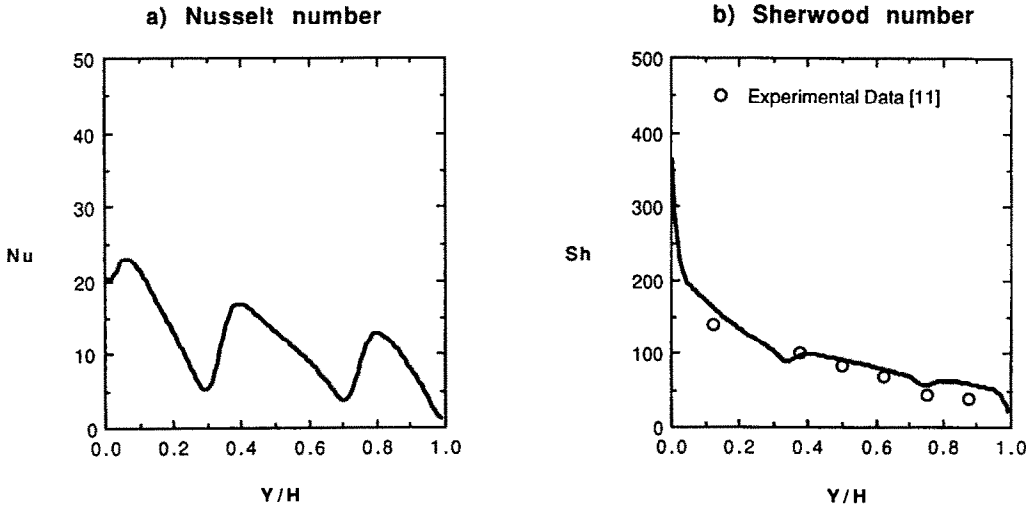

FIG. 6. Local Nusselt and Sherwood number distributions along the vertical heated plate: $Gr_T = 3 \times 10^5$, $Gr_M = 3 \times 10^6$.

faces used in the experiments. The assumption of uniform concentration may not be appropriate for an electrochemical experiment in a stratified fluid in an enclosure.

4.3. *Effect of buoyancy ratio on flow structures and transfer rates*

With the solutal Grashof number fixed at 10^5, various thermal Grashof numbers are superimposed either for opposing or aiding buoyancy. Streamline plots for different opposing buoyancy conditions are shown in Fig. 7 as a function of buoyancy ratio. For $|Gr_T| < 10^4$, solutal buoyancy is dominant. The overall structure is unicellular motion rotating in the clockwise direction, which is similar to the pure solutal convection shown in Fig. 7(a). For $|Gr_T| > 5 \times 10^4$, thermal buoyancy is dominant. The overall flow structure is again a unicell motion rotating in the counterclockwise direction driven by thermal buoyancy. Compared to pure thermal convection, however, there are separation points near the bottom of the cold wall (left wall) and near the top of the hot wall. In the recirculation zones, the flow recirculates very slowly in the opposite direction driven by the solutal buoyancy. The streamlines of pure thermal convection, $Gr_M = 0$, are shown in Fig. 7(e) for reference. The boundary layer is much thicker than that of pure solutal convection, since the more-diffusive species (heat) is dominant.

For a range of Grashof number ratios between -10 and -2, thermal and solutal forces are of the same order of magnitude. It could have been expected to have a transitional buoyancy ratio at which the flow direction is reversed. However, streamlines in Fig. 7(c) show a three-cell flow structure generated for $N = -5$ ($Gr_T = 2 \times 10^{-4}$). Each cell rotates counter-clockwise driven by the thermal buoyant force. The thermal buoyant forces from the side walls overcome the shear stress between cells which rotate the fluid in each cell in the same direction. Small idling cells rotating clockwise can be observed between cells and walls.

Streamline plots for various aiding buoyancy conditions are shown in Fig. 8. Figure 8(a) is a streamline plot at $Gr_T = 10^3$, and shows a unicell flow structure rotating clockwise. For the mildly aiding condition with a small Gr_T superimposed, the results are similar to pure solutal convection as was shown in Fig. 7(a). Figure 8(e) shows streamlines at $Gr_M = 1.5 \times 10^4$. Even though the magnitude of Gr_T is smaller than Gr_M ($N = 6.67$), the thermal buoyancy is dominant over the solutal one. The overall flow is unicellular motion similar to pure thermal convection as shown in Fig. 7(e), but rotating in the opposite direction. For $10 < N < 50$, three cell flow structures are obtained again (Figs. 8(b)–(d)). The range of N for the three cell flow structure in the aiding buoyancy conditions is found to be larger compared to the opposing buoyancy conditions.

The overall Nusselt number is shown in Fig. 9(a) as a function of Gr_T. The results for both aiding and

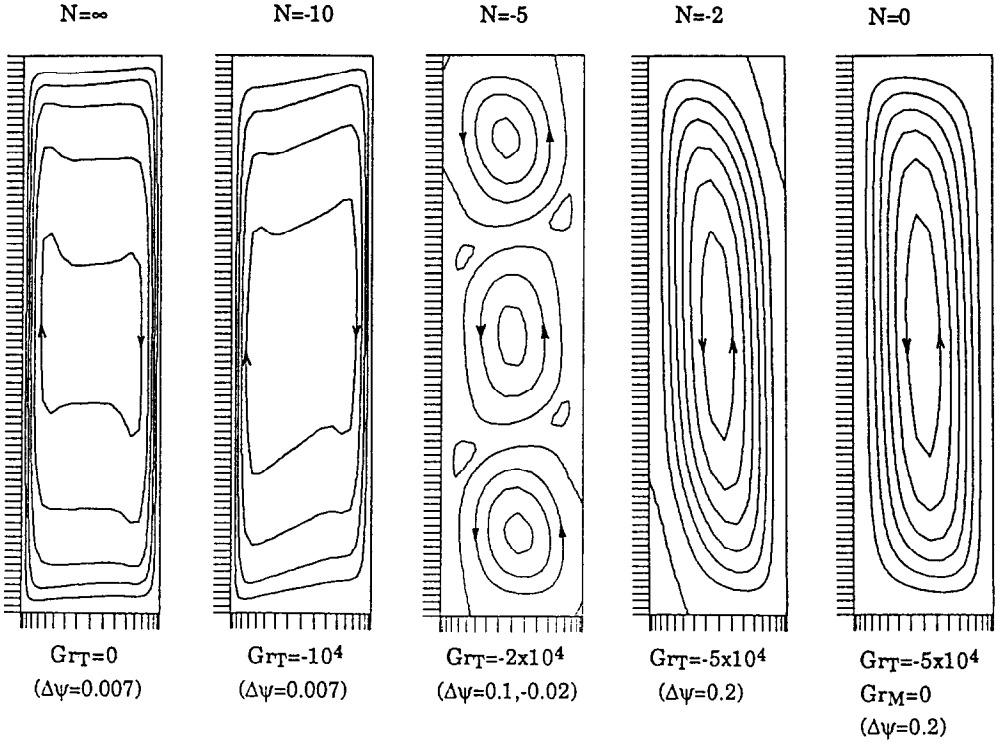

FIG. 7. Streamline plots for opposing buoyancy conditions: $Gr_M = 10^5$.

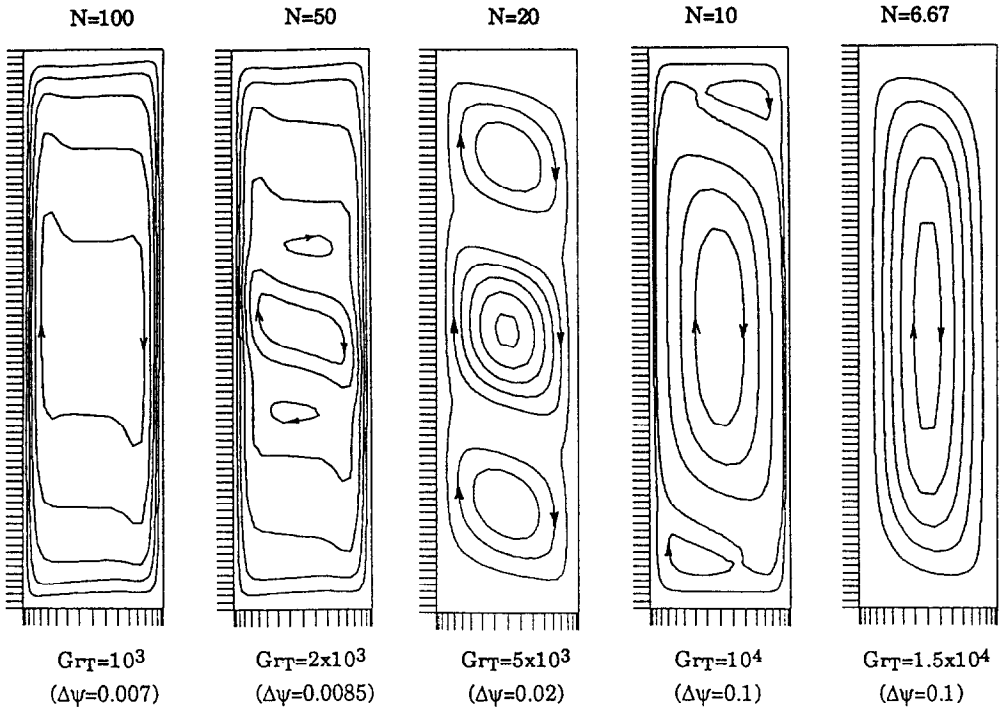

FIG. 8. Streamline plots for aiding buoyancy conditions: $Gr_M = 10^5$.

opposing flow conditions are superimposed with the pure heat transfer results shown with a dotted line. As the thermal Grashof number increases, the Nusselt numbers for both aiding and opposing buoyancy conditions converge to the dotted line. In the other limit ($Gr_T = 0$), the Nusselt number approaches the value of pure conduction, which is 4. The overall Nusselt number for negative Gr_T is reduced compared to the pure heat transfer results in the intermediate range of buoyancy ratios. It is interesting to note that the Nusselt number is also decreased slightly even for positive Gr_T in the intermediate range of buoyancy ratios compared to the pure heat transfer case. This is due to the multicell flow structure explained earlier. However, the effect of the superimposed Gr_M on the overall Nusselt number appears to be very weak in the present range of parameters. In Fig. 9(b), the overall Sherwood number is presented as a function of thermal Grashof number for aiding and opposing buoyancy conditions. The dotted line here indicates accompanied mass transfer rates due to a purely thermal-driven convection flow (not pure mass transfer convection). Over the entire range of Gr_T, the Sherwood number for the opposing buoyancy condition is observed to be smaller than that for the aiding buoyancy condition.

4.4. *Parametric map of double diffusive convection*

Figure 10 shows the parametric plane of *Le*–*N*, the ratio of two diffusivities vs the ratio of two buoyant forces, for cavities with an aspect ratio, $H/L = 4$, in laminar boundary layer flow. Positive N corresponds to aiding flow, and negative N corresponds to opposing flow. Pure heat transfer falls on the line $N = 0$, and pure mass transfer falls on the lines $N = \pm\infty$. Along the line $Le = 1$, where both diffusivities are equal, the resulting buoyant force is a direct sum of the two buoyant forces. The point shown ($N = -1$, $Le = 1$) is a theoretical point where there is no motion at all. The map should be the same for $1/Le$–$1/N$ coordinates, because of the interchangeability of the roles of Pr–Sc and Gr_T–Gr_M.

The shaded area shows the approximate range of multicell flow regions, based on the present numerical results. A multicell structure is possible only when the Lewis number is much different from unity. For the Lewis number close to unity, between 1 and 10, a unicell flow structure is obtained, the direction of which is determined by the buoyancy ratio. Moreover, the solutal Grashof number should be larger than the thermal Grashof number in magnitude in order to obtain a multicell structure. In thin concentration boundary layers, the solutal buoyant force should overcome the thermal buoyant force in the opposite direction and the resulting shear force by the flow. The range of the multicell region depends on the individual magnitudes of Grashof numbers as well as their ratio. In order to define the boundaries of different flow regimes more clearly, more results are needed in other ranges of the governing parameters.

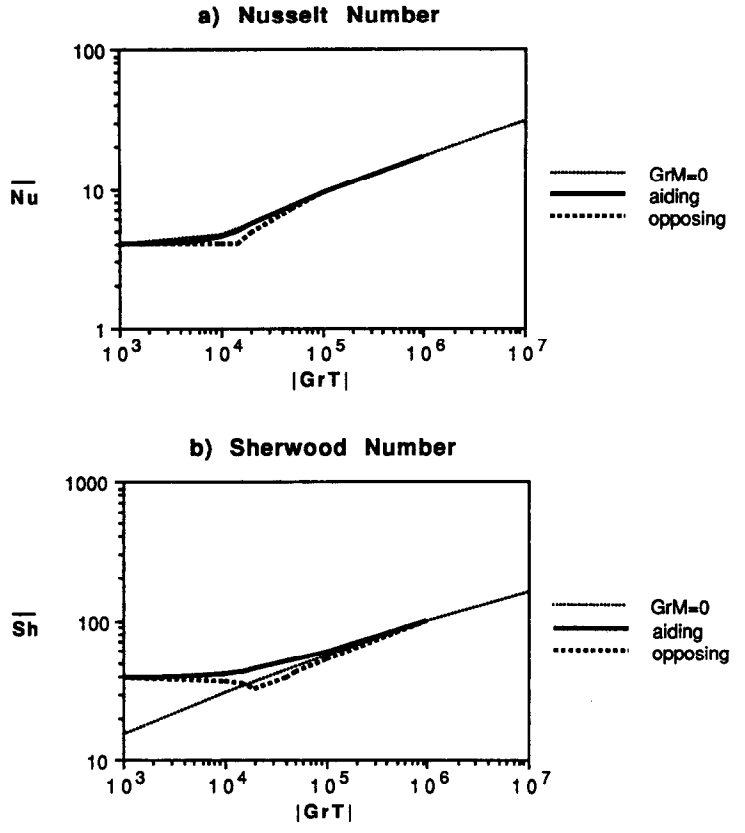

FIG. 9. Overall Nusselt and Sherwood numbers as a function of Gr_T: $Gr_M = 10^5$.

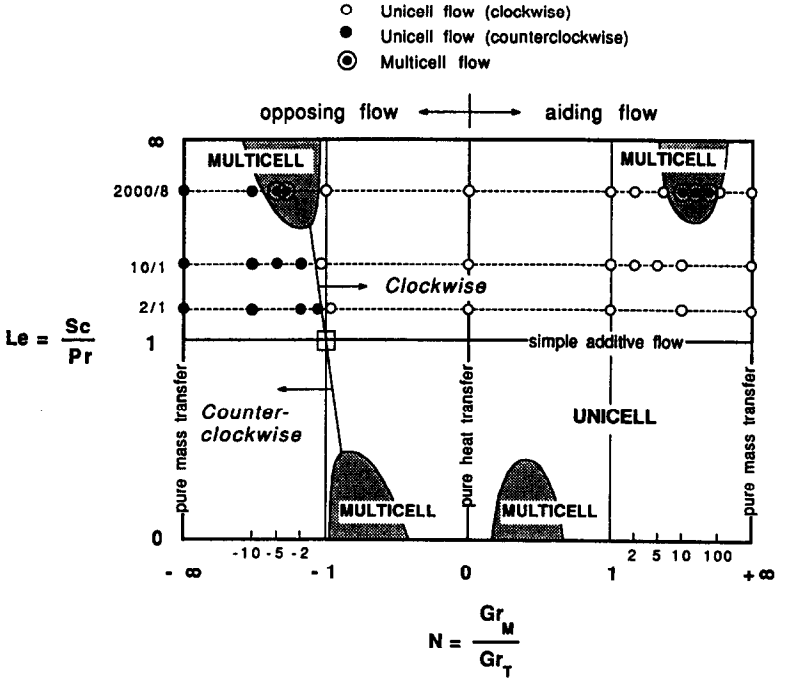

FIG. 10. Double diffusive flow regime plot: $H/L = 4$, $Gr_M = 10^5$.

5. CONCLUSIONS

Double diffusive natural convection flows have been investigated for various conditions in a vertical rectangular cavity with an aspect ratio of 4. The flow regimes can be categorized as thermally dominant, solutally dominant, and equally important. The thermally dominant and solutally dominant convection results in unicell flow structures as in pure thermal or pure solutal convection. In the intermediate range of Grashof number ratio, a multicell flow structure is obtained regardless of the direction of the buoyant forces for a high Lewis number. The minimum Lewis number resulting in a multicell flow structure is yet to be determined.

The characteristics of the multicell flow structure have been given in detail. The flow direction in the thin concentration boundary layer does not appear to affect the overall flow structure significantly. The temperature and concentration profiles in the cavity are unique to double diffusive natural convection. The peculiar Nusselt number and Sherwood number distributions along the vertical walls are also due to the double diffusive multicell flow structure. The present numerical results agree with corresponding experimental results reasonably well.

Numerical solutions require a very fine mesh to resolve the thin concentration boundary layers and the thin interfaces between cells because of the small solutal diffusivity. The grid spacing is found to not only affect the accuracy of the overall heat and mass transfer rates but also affect the flow structure in the converged solution.

Acknowledgements—This work is partially supported by a grant from the Minnesota Supercomputer Institute of the University of Minnesota.

REFERENCES

1. J. S. Turner, *Buoyancy Effects in Fluids*. Cambridge University Press, London (1979).
2. S. Ostrach, Fluid mechanics in crystal growth—The 1982 Freeman Scholar Lecture, *J. Fluids Engng* **105**, 5–20 (1983).
3. S. Clark, F. J. Spera and D. A. Yuen, Steady state double-diffusive convection in magma chambers heated from below, University of Minnesota Supercomputer Institute Report UMSI 86/39 (1986).
4. J. C. Heinrich, A finite element model for double diffusive convection, *Int. J. Numer. Meth. Engng* **20**, 447–464 (1984).
5. C. F. Chen, D. G. Briggs and R. A. Wirtz, Stability of thermal convection in a salinity gradient due to lateral heating, *Int. J. Heat Mass Transfer* **14**, 57–65 (1971).
6. C. Beckermann and R. Viskanta, Double-diffusive convection during dendritic solidification of a binary mixture, *PhysicoChem. Hydrodyn.* **10**, 195–213 (1988).
7. C. Y. Hu and M. M. El-Wakil, Simultaneous heat and mass transfer in a rectangular cavity, *Proc. 5th Int. Heat Transfer Conf.*, Vol. 5, pp. 24–28 (1974).
8. C. Benard, D. Gobin and J. Thevenin, Thermosolutal natural convection in a rectangular enclosure: numerical results. In *Heat Transfer in Convective Flows* (Edited by R. K. Shah), ASME HTD-Vol. 107, pp. 249–254 (1989).
9. Y. Kamotani, L. W. Wang, S. Ostrach and H. D. Jiang, Experimental study of natural convection in shallow enclosures with horizontal temperature and concentration gradients, *Int. J. Heat Mass Transfer* **28**, 165–173 (1985).
10. J. Lee, M. T. Hyun and K. W. Kim, Natural convection in confined fluids with combined horizontal temperature and concentration gradients, *Int. J. Heat Mass Transfer* **31**, 1969–1977 (1988).
11. H. Han and T. H. Kuehn, Double diffusive natural convection in a vertical rectangular enclosure—I. Experimental study, *Int. J. Heat Mass Transfer* **34**, 449–459 (1991).
12. H. Han, Double diffusive natural convection in a vertical rectangular enclosure, Ph.D. Thesis, University of Minnesota (1988).
13. S. V. Patankar, *Numerical Heat Transfer and Fluid Flow*. Hemisphere, Washington, DC (1980).
14. G. de Vahl Davis, Natural convection of air in a square cavity: a benchmark numerical solution, *Int. J. Numer. Meth. Fluids* **3**, 249–264 (1983).

CONVECTION NATURELLE DOUBLEMENT DIFFUSIVE DANS UNE CAVITE RECTANGULAIRE VERTICALE—II. ETUDE NUMERIQUE

Résumé—On étudie numériquement l'écoulement de convection naturelle doublement diffusive dans une cavité rectangulaire verticale, de rapport de forme 4, quand les gradients de température et de concentration sont imposés dans la direction horizontale. Un algorithme aux différences finies est adopté pour résoudre les équations non linéaires de quantité de mouvement couplées avec celles de l'énergie et de la concentration. Les structures multicellulaires de l'écoulement observées expérimentalement par les auteurs sont simulées avec succès. Différents régimes de structure d'écoulement sont obtenus en fonction du rapport des nombres de Grashof pour des conditions de flottement aidées ou opposées.

DOPPELT-DIFFUSIVE NATÜRLICHE KONVEKTION IN EINEM SENKRECHTEN RECHTECKIGEN HOHLRAUM—II. NUMERISCHE UNTERSUCHUNG

Zusammenfassung—Die doppelt-diffusive natürliche Konvektionsströmung in einem senkrechten rechteckigen Hohlraum mit dem Seitenverhältnis 4 wird numerisch untersucht, wobei Temperatur- und Konzentrationsgradienten in waagerechter Richtung aufgeprägt werden. Die nicht-linearen Impulsgleichungen, die mit der Energie- und der Konzentrationsgleichung gekoppelt sind, werden mit Hilfe eines Finite-Differenzen-Verfahrens gelöst. Die von den Autoren im Experiment beobachteten multizellularen Strömungsstrukturen bei doppelt-diffusiver Konvektion ergeben sich auch in der Berechnung. Es zeigen sich Bereiche mit unterschiedlicher Strömungsstruktur, abhängig vom Verhältnis der Grashof-Zahlen bei gleichgerichteter und gegengerichteter thermischer und konzentrationsbedingter Auftriebsströmung.

КОНВЕКЦИЯ С ДИФФУЗИЕЙ ТЕПЛА И МАССЫ В ВЕРТИКАЛЬНОЙ ПРЯМОУГОЛЬНОЙ ПОЛОСТИ—II. ЧИСЛЕННОЕ ИССЛЕДОВАНИЕ

Аннотация—Численно исследуется естественноконвективное течение жидкости с диффузией тепла и массы в вертикальной прямоугольной полости с отношением сторон, равным 4, при наложении температурных и концентрационных градиентов направленных горизонтально. Для решения нелинейных уравнений сохранения количества движения, совместно с уравнениями сохранения энергии и массы, используется метод конечных разностей. Успешно моделируются экспериментально наблюдавшиеся авторами многоячеистые структуры течения в зависимости от отношения чисел Грасгофа для спутно и противоположно направленных подъемных сил.